

Synthesis, structural and optical characterization of Ni-doped ZnO nanoparticles

R. Elilarassi · G. Chandrasekaran

Received: 12 May 2010 / Accepted: 25 August 2010 / Published online: 7 September 2010
© Springer Science+Business Media, LLC 2010

Abstract Nanocrystalline $\text{Zn}_{1-x}\text{Ni}_x\text{O}$ ($x = 0.00, 0.02, 0.04, 0.06, 0.08$) powders were synthesized by a simple sol-gel autocombustion method using metal nitrates of zinc, nickel and glycine. Structural and optical properties of the Ni-doped ZnO samples annealed at 800 °C are characterized using X-ray diffraction (XRD), scanning electron microscopy (SEM), energy dispersive analysis using X-rays (EDAX), UV-visible spectroscopy and photoluminescence (PL). X-ray diffraction analysis reveals that the Ni-doped ZnO crystallizes in a hexagonal wurtzite structure and secondary phase (NiO) was observed with the sensitivity of XRD measurement with the increasing nickel concentration ($x \geq 0.04$). The lattice constants of Ni-doped ZnO nanoparticles increase slightly when Ni^{2+} is doped into ZnO lattice. The optical absorption band edge of the nickel doped samples was observed above 387 nm (3.20 eV) along with well-defined absorbance peaks at around 439 (2.82 eV), 615 (2.01 eV) and 655 nm (1.89 eV). PL measurements of Ni-doped samples illustrated the strong UV emission band at ~ 3.02 eV, weak blue emission bands at 2.82 and 2.75 eV, and a strong green emission band at 2.26 eV. The observed red shift in the band gap from UV-visible analysis and near band edge UV emission with Ni doping may be considered to be related to the incorporation of Ni ions into the Zn site of the ZnO lattice.

1 Introduction

In the recent years, semiconductor nanomaterials have attracted much attention due to their potential technological applications such as storage devices, optoelectronics, nanoelectronics and photonic devices [1–5]. Diluted magnetic semiconductors (DMS) are semi-conducting alloys with spin carriers in addition to charge carriers as an added degree of freedom in a single substance prepared by dilute substitution of transition metal (TM) ions in the semiconductor host material. DMS have been focused on a new practical technology namely spin-electronics or spintronics [6, 7]. The advantages of such spin based electronic devices include enabling of instant-on computer, higher data processing speed, increased integration density, very low electrical energy consumption. There has been an intense search for inherent wide band-gap-oxide-based DMS systems ever since the theoretical prediction of ferromagnetism above room temperature in TM doped ZnO based DMS [8]. TM doped ZnO exhibits multifunctional properties like magnetic, semi-conducting and optical properties coexisting in a single material. Also, the TM doping into ZnO offers a possible means of tuning the band gap to make use in optoelectronic applications such as light emitters and UV detectors.

An oxide based DMS employs a nonmagnetic oxide semiconductor material like ZnO or TiO_2 as the host which is doped with TM. ZnO is an efficient II–VI semiconductor material crystallizes in the wurtzite structure with the lattice constants $a = 3.24 \text{ \AA}$ and $c = 5.20 \text{ \AA}$ having a direct bandgap (as wide as 3.37 eV), similar to that of GaN. ZnO is optically transparent material with a large exciton binding energy of 60 MeV. In recent years, ZnO doped with TMs has been the subject of much attention because of its potential for important applications such transparent

R. Elilarassi (✉) · G. Chandrasekaran
Department of Physics, Magnetsim and Magnetic Materials Lab,
School of Physical, Chemical and Applied Sciences, Pondicherry
University, Puducherry 605 014, India
e-mail: ezhil1984_r@yahoo.co.uk

conductors, heterojunction solar cells, gas sensors, surface acoustic waves, piezoelectric devices, antireflection coatings, etc. [9–15]. Both experimental and theoretical research is underway and there has been a great deal of focus on the TM doped ZnO based DMS for their potential application in spintronics devices [16–20].

Theoretical calculations predict that stable ferromagnetism could be achieved in the TM (Ni-, V-, Mn, Fe-, Cr- or Co-) doped ZnO, even in the absence of additional carrier doping [21]. Li et al. [22], reported that the $Zn_{1-x}Ni_xO$ powders prepared by sol-gel method, Ni dopant substitutes for Zn only up to 5%. It was reported that, in TM doped ZnO, the evolution of secondary phases emerging out of dopant material along with the single phase $Zn_{1-x}TM_xO$ was strongly related to growth temperature and doping concentration [23]. In the present paper, the synthesis of nickel doped ZnO nanoparticles using sol-gel auto-combustion method and their structural and optical characterizations are discussed in detail.

2 Experimental procedure

Nanocrystalline $Zn_{1-x}Ni_xO$ ($x = 0.00, 0.02, 0.04, 0.06$ and 0.08) powder samples were synthesized by a simple and low-temperature sol-gel auto-combustion method. All chemicals used were of analytical grade purity. In a typical synthesis of $Zn_{1-x}Ni_xO$ samples, the appropriate proportion of $Zn(NO_3)_2 \cdot 6H_2O$, $Ni(NO_3)_2 \cdot 6H_2O$, and $C_2H_5NO_2$ (glycine) were completely dissolved in a 1,000 mL beaker to obtain a 100 mL aqueous solution. The aqueous solution was then stirred for about 1 h in order to mix the solution uniformly. The mixed precursor solution was evaporated on a hot plate at $100^\circ C$ under constant stirring and was concentrated by heating until the excess free water gets evaporated. Then, the solution converted into a “gel”. The “gel” was subsequently swelling into foam and underwent a strong self-propagating combustion reaction to give a fine powder. The resulting powders of undoped ZnO were milky white in colour. Nickel doped samples were moss green and became darker with increasing Ni content. All the samples were grinded for an hour and were prepared as pellets. The pellets were subjected to annealing at $800^\circ C$ for 8 h and used for further characterization studies.

The crystalline nature and the phase purity of the undoped and nickel doped ZnO powder samples were examined by X-ray powder diffraction analysis (XRD) using PANalytical Model: X’Pert PRO (Cu $K\alpha$ radiation, $\lambda = 1.54, 178 \text{ \AA}$). The mean crystallite sizes were estimated using the Scherer Equation, and the lattice constants were obtained using the XRD data. The microstructure of the resulting nanopowders was characterized using HIT-ACHI Model: S-3,400 N scanning electron microscope.

Room temperature optical absorption spectra of the samples were recorded in the 200–800 nm ranges using a Varian Cary 5000 UV–vis–NIR Spectrophotometer. Room temperature photoluminescence spectra of the samples were recorded using a spectrofluorimeter (Fluorolog-3) to characterize the optical emission properties of the samples.

3 Results and discussion

3.1 Structural characterization

The crystal structure and phase purity of as-prepared undoped ZnO and different composition of Ni-doped ZnO nanoparticles annealed at $800^\circ C$ were characterized using X-ray diffraction. Figure 1 shows a typical XRD spectrum of pure ZnO and $Zn_{1-x}Ni_xO$ ($x = 0.02, 0.04, 0.06, 0.08$) nanoparticles annealed at $800^\circ C$. XRD pattern reveals that the diffraction peaks of undoped ZnO and nickel doped ZnO nanoparticles can be indexed to hexagonal wurtzite structure of ZnO which are in good agreement with the standard JCPDS file for ZnO (JCPDS36-1451, $a = 3.249 \text{ \AA}$, $c = 5.206 \text{ \AA}$ having space group P63mc). When the content of Ni(x) is 0.02, no trace of nickel metal, oxides, or any binary zinc nickel phases is observed, however, when $x \geq 0.04$, a new phase emerges at ($2\theta \sim 42.9^\circ$) as shown in Fig. 1. Such an additional diffraction peak corresponds to the secondary phase of NiO (2 0 0) (matched with JCPDS 78-0643). The intensity of NiO peak increases with increasing nickel concentration indicating that phase segregation has occurred and the lower solubility limit of Ni in $Zn_{1-x}Ni_xO$ nanoparticles is ($x < 0.04$). Such a structural degradation in the ZnO lattice may be attributed to introduction of a foreign impurity with subsequent annealing [24].

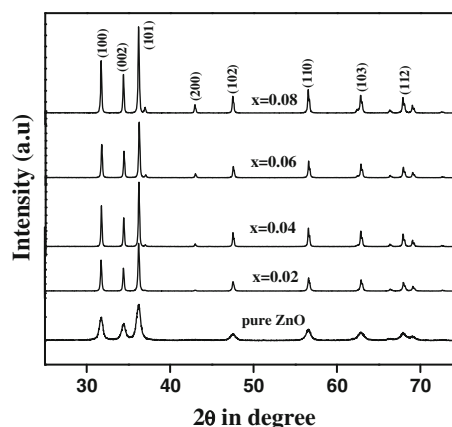


Fig. 1 XRD pattern of as-prepared ZnO and nickel doped ZnO nanoparticles annealed at $800^\circ C$

The average crystallite size of the nickel doped ZnO powders were estimated from X-ray line broadening using the Debye–Scherrer’s equation

$$D_{h,k,l} = 0.9\lambda/(\Delta\theta \cos \theta) \tag{1}$$

D —average crystallite diameter, λ is the wavelength of X-ray radiation, $\Delta\theta$ -full width at half maximum (FWHM) and θ is the Bragg angle. Figure 2 shows the variation of crystallite size with nickel concentration. The crystallite size of the samples increases with increasing Ni content, however a sudden increase in crystallite size of nickel doped samples annealed from that of as-prepared pure ZnO may be due to the annealing treatment of the samples at 800 °C. Such variation in particle size is evident from Fig. 1 that pure ZnO exhibits broad diffraction peaks when compared to that of nickel doped samples. The lattice parameters a and c of the samples are calculated using the formula:

$$\sin^2 \theta = \frac{\lambda^2}{4} \left[\frac{4}{3} \left(\frac{h^2 + hk + k^2}{a^2} \right) + \frac{l^2}{c^2} \right] \tag{2}$$

θ is the diffraction angle, λ is incident wavelength ($\lambda = 0.15406$ nm) and h, k and l are all Miller indices. Table 1 shows that the lattice constants a and c of nickel doped ZnO nanoparticles are slightly larger than those of pure ZnO, because the ionic radius of Ni^{2+} (0.68 Å) is

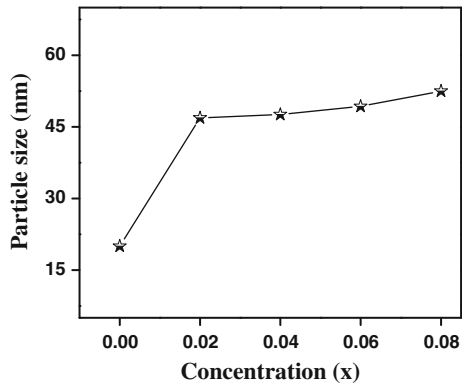


Fig. 2 Variation of particle size as-prepared ZnO and nickel doped ZnO nanoparticles annealed at 800 °C

Table 1 Variation of lattice constants with different concentration of nickel doped ZnO nanoparticles

Samples annealed at 800 °C (x)	Lattice constants (Å)	
	a	c
ZnO	3.2480	5.2075
$\text{Zn}_{0.98}\text{Ni}_{0.02}\text{O}$	3.2488	5.2086
$\text{Zn}_{0.96}\text{Ni}_{0.04}\text{O}$	3.2509	5.2104
$\text{Zn}_{0.94}\text{Ni}_{0.06}\text{O}$	3.2533	5.2127
$\text{Zn}_{0.92}\text{Ni}_{0.08}\text{O}$	3.2547	5.2143

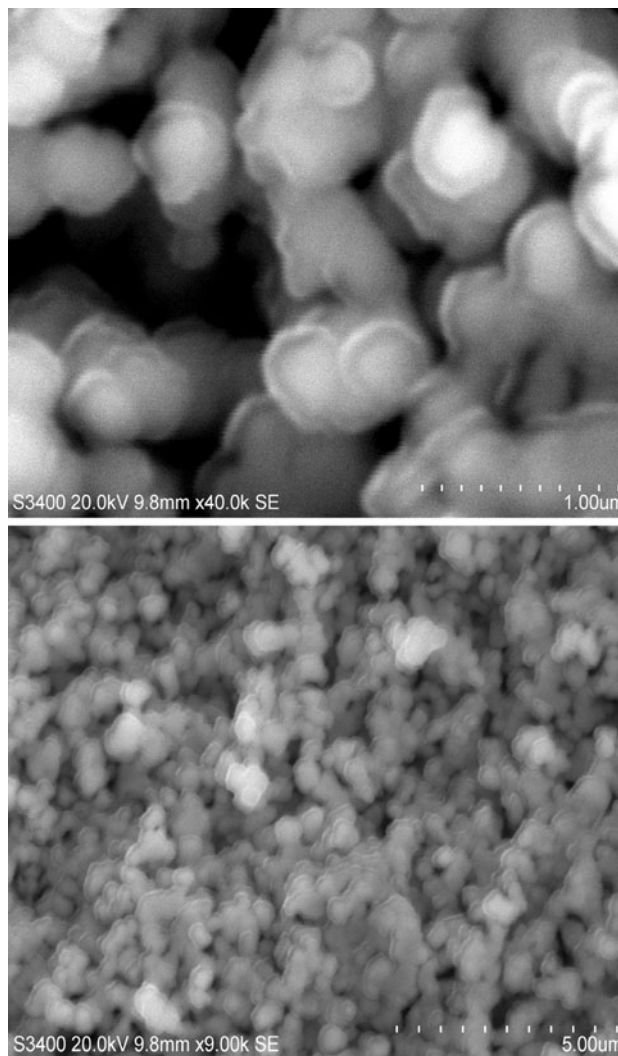


Fig. 3 SEM micrographs of $\text{Zn}_{0.98}\text{Ni}_{0.02}\text{O}$ sample annealed at 800 °C

larger than that of Zn^{2+} (0.60 Å). The expansion of the lattice constants of Ni-doped ZnO nanoparticles indicated that Ni ions systematically substituted Zn ions into the ZnO structure [25]. Morphology of the $\text{Zn}_{1-x}\text{Ni}_x\text{O}$ ($x = 0.02$) nanoparticles investigated using scanning electron microscopy is shown in Fig. 3. The SEM images of the sample shows the presence of evenly distributed spherical nanoparticles with particle size ranging ~400 nm.

3.2 Optical characterization

The effect of Ni doping concentration on the band gap of ZnO and substitution of Ni^{2+} ions in tetrahedral sites of wurtzite structure of ZnO was further confirmed using UV–visible optical spectroscopy measured in the range 300–800 nm. Inset of Fig. 4 shows the room temperature optical absorption spectra of the as-prepared undoped ZnO and nickel doped ZnO nanoparticles annealed at 800 °C.

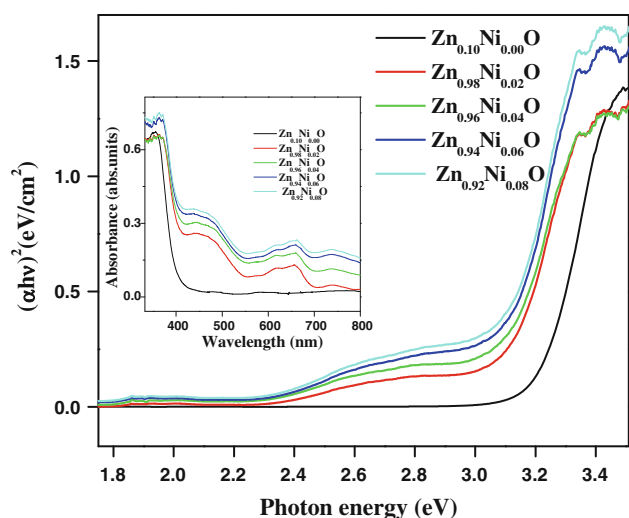


Fig. 4 Photon energy versus $(\alpha hv)^2$ of as-prepared ZnO and nickel doped ZnO nanoparticles annealed at 800 °C. Inset figure shows the UV–vis absorption spectra of as-prepared ZnO and nickel doped ZnO nanoparticles annealed at 800 °C

The absorption band edge of undoped ZnO is observed at 387 nm and it gets shifted to longer wavelength region for the Ni-doped ZnO samples. The observed red shift in the absorption band edge with nickel doping in ZnO may be due to the sp-d exchange interactions between the band electrons and the localized d-electrons of the Ni²⁺ ions. Such a red shift in band edge with increasing nickel dopant is a clear indication for the incorporation of Ni ions into the Zn site of the ZnO lattice [26–28]. In addition to absorption band edge, TM doped ZnO samples mostly exhibit absorption peaks in the visible region. It is observed that the absorption spectrum of nickel doped ZnO nanoparticles shows additional absorption bands corresponding to *d–d* transitions at 439 (2.82 eV), 615 (2.01 eV) and 655 nm (1.89 eV). Such mid band gap states can be assigned as characteristic of Ni²⁺ with tetrahedral symmetry [29]. Two absorption peaks at 1.89 and 2.02 eV can be clearly seen. These absorption bands may be ascribed to the $^4A_2(F) \rightarrow ^3T_1(P)$ crystal field transitions in tetrahedrally bonded Ni²⁺ ions [30–32].

The absorption coefficient and the band gap energy can be described by the following equation

$$\alpha hv = A(hv - E_g)^{1/2} \quad (3)$$

where $h\nu$ is the incident photon energy, E_g is the band gap energy and A is a constant. A plot of $(\alpha hv)^2$ versus $h\nu$ is made to determine E_g using the linear fit process. The extrapolated absorption thresholds of the undoped and Ni-doped ZnO nanoparticles are shown in Fig. 4. It reflects the band gap energies of the corresponding samples and indicates that a red shift in the band gap have occurred with nickel doping. The red shift in the band gap with increasing

nickel dopant could be interpreted mainly due to the sp–d exchange interactions between the band electrons and the localized d electrons of the Ni²⁺ ions substituting Zn ions. Such electronic transitions observed in all the nickel doped samples indicating the substitution of Ni²⁺ cations for the Zn²⁺ ions at the ZnO lattice site tetrahedrally. The red shift in the absorption band edge and the observed electronic transitions of Ni²⁺ clearly indicates the incorporation of Ni ions inside ZnO lattice. Thus, Ni ions exist in a tetrahedral crystal field in the +2 state without changing the wurtzite crystal structure of ZnO.

Room temperature photoluminescence (PL) spectra of Ni-doped ZnO samples were measured using spectrofluorimeter (Fluorolog-3) excited with a Xe-lamp light source (350 nm) under identical excitation wavelength 370–575 nm. Figure 5 shows the PL spectra of the as-prepared undoped ZnO and Ni doped ZnO nanoparticles annealed at 800 °C. It consist of a strong UV emission peak which is centered at ~410 nm (~3.01 eV) and weak blue emission peaks centered at 450 (2.75 eV) and 468 nm (2.65 eV) and a strong green emission band centered at 547 nm (2.26 eV), respectively., The UV emission intensity dominates when compared to that of defect related visible emission and it gets reduced significantly with nickel doping. In general, visible emissions are referred to as deep-level emission and attributed to the recombination of electrons deeply trapped in oxygen vacancies and zinc interstitials, with photogenerated holes. The visible emissions observed may be ascribed to the intrinsic defects and oxygen vacancies [33, 34], but the exact mechanism responsible for these emissions are still in debate. The blue emission around 468 (2.65 eV) and 440 nm (2.82 eV) can be assigned to intrinsic defects, particularly interstitial zinc

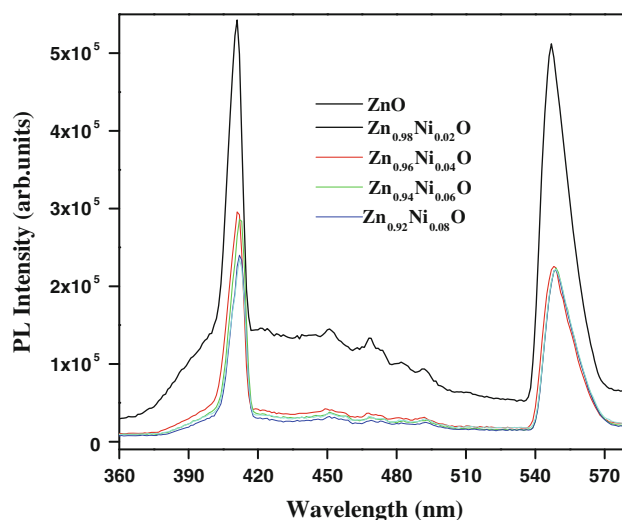


Fig. 5 Photoluminescence spectra of undoped and nickel doped ZnO nanoparticles annealed at 800 °C. Inset of the figure shows the red shift in UV emission with Ni-doping

(Zn_i) may be originated from the radiative overlap of the electrons transition from the shallow donor level of oxygen vacancies and from the defect donor level associated with ionized oxygen vacancies to the valence band [35]. The green emission observed at 547 nm (2.26 eV) is commonly attributed to the transition of a photo-generated electron from a dark level below the conduction band to a deeply trapped hole resulting from an oxygen vacancy [36]. With increasing Ni content in ZnO, the probability of recombination of electrons and holes in the valence band has reduced which results in a slight decrease in the green emission intensity in nickel doped samples from that of pure ZnO.

The strong UV emission peak centered at ~410 nm (~3.01 eV) in undoped and Ni-doped ZnO nanoparticles most likely originates from the unsaturated Zn sites in the ZnO or the formation of band tailing in the band gap, which is often induced by the introduction of impurity into the semiconductor [37–39] slightly shift towards the longer-wavelength with nickel doping as shown in Fig. 5. It is clear from Fig. 6 that the band gap of near band edge UV emission decreases with nickel doping indicates the red-shift of band gap, which is similar to the results of Zhao et al. [40]. Inset of Fig. 6 shows the red shift in the UV band gap with increasing nickel dopant in ZnO which is in agreement with the red shift of near band edge UV emission as shown in Fig. 6. This could be interpreted to be mainly due to the sp–d exchange interactions between the band electrons and the localized d electrons of the Ni²⁺ ions substituting Zn ions [41–43]. The observed red-shift of band gap with nickel doping suggesting possible doping of Ni²⁺ into the ZnO lattice may induce band edge bending. It

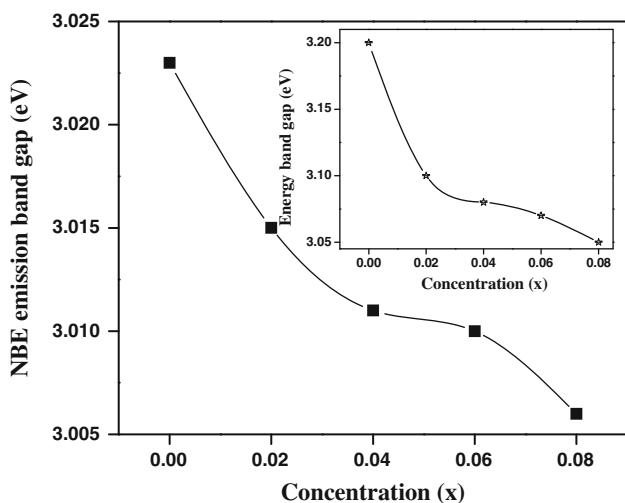


Fig. 6 Variation of near band edge UV emission band gap of undoped and nickel ZnO nanoparticles annealed at 800 °C. *Inset* shows the band gap variation of the samples from UV–visible measurements

is suggested that with nickel doping more defect states occurs below the conduction band, which makes some of the excited electrons in the conduction band to get relax to the defect states. Such a process may be attributed to the decrease in UV emission intensity consecutively. A slight decrease in visible emission intensity may be attributed due to the addition of nickel or due to annealing of the samples or due to the reduction of defect states.

4 Conclusions

Undoped ZnO and nickel doped ZnO nanoparticles have been successfully synthesized using sol–gel auto-combustion method. The structural study reveals that annealed samples show the existence of secondary phase NiO in the samples $x \geq 0.04$. A red shift in the band gap has been observed from the room temperature optical absorption and PL spectra of nickel doped ZnO nanoparticles. Such a red shift in band gap may be attributed to the sp–d exchange interactions between the band electrons and the localized d electrons of the Ni²⁺ ions substituting Zn ions clearly indicating the incorporation of Ni ions into the Zn site of the ZnO lattice. Magnetic properties of the samples are yet to be studied. Thus, from the excellent structural and optical properties of the samples, we expect that nickel doped ZnO nanoparticles could be an efficient material for spintronics applications.

Acknowledgments The authors are very thankful to central instrumentation facility, Pondicherry University for providing SEM and PL studies, UGC for funding XRD measurement at Department of Physics, Pondicherry University, and Dr. R. Venkatesan for providing UV–visible spectroscopic analysis, Department of Chemistry, Pondicherry University, Puducherry, India.

References

1. A. Miyake, H. Kominami, H. Tatsuoka, H. Kuwabara, Y. Nak-aushi, Y. Hatanaka, *J. Cryst. Growth* **294**, 214 (2000)
2. J. Hu, T.W. Odom, C.M. Lieber, *Acc. Chem. Res.* **32**, 435 (1999)
3. C.A. Mirkin, *Science* **286**, 2095 (1999)
4. S.M. Prokes, K.L. Wang, *Mater. Res. Sci. Bull.* **24**, 13 (1999)
5. S. Nakamura, *Science* **281**, 956 (1998)
6. H. Ohno, *Science* **281**, 951 (1998)
7. Y. Matsumoto, M. Murakami, T. Shono, T. Hasegawa, T. Fukumura, M. Kawasaki, P. Ahmet, T. Chikyow, S. Koshihara, H. Koinuma, *Science* **291**, 854 (2001)
8. T. Dietl, H. Ohno, F. Matsukura, J. Cibert, D. Ferrand, *Science* **287**, 1019 (2000)
9. M.A. Martinez, J. Herrero, M.T. Gutierrez, *Sol. Energy Mater. Sol. Cells* **45**, 75 (1997)
10. D. Song, A.G. Aberle, J. Xia *Appl. Surf. Sci.* **195**, 291 (2002)
11. O.I. Lupan, S.T. Shishiyanu, T.S. Shishiyanu, *Superlatt. Microstruct.* **42**, 375 (2007)
12. X.L. Cheng, H. Zhao, L.H. Huo, S. Gao, J.G. Zhao, *Sens. Actuators B* **102**, 248 (2004)

13. H.S. Kang, J.S. Kang, J.W. Kim, S.Y. Lee, *J. Appl. Phys.* **95**, 1246 (2004)
14. S.C. Ko, Y.C. Kim, S.S. Lee, S.H. Choi, S.R. Kim, *Sens. Actuators A* **103**, 130 (2003)
15. S. Major, K.L. Chopra, *Sol. Energy Mater.* **17**, 319 (1988)
16. M. Lorenz, E.M. Kaidashev, A. Rahm, T. Nobis, J. Lenzner, G. Wagner, D. Spemann, H. Hochmuth, M. Grundmann, *Appl. Phys. Lett.* **86**, 143113 (2005)
17. K. Ueda, H. Tabota, T. Kamai, *Appl. Phys. Lett.* **79**, 988 (2001)
18. J.F. Gregg, I. Petej, E. Jouguelet, C. Dennis, *J. Phys. D Appl. Phys.* **35**, R121 (2002)
19. R. Janisch, P. Gopal, N.A. Spaldin, *J. Phys.: Condens. Matter* **17**, R657 (2005)
20. T. Fukumura, H. Toyosaki, Y. Yamada, *Semicond. Sci. Technol.* **20**, S103 (2005)
21. T. Wakano, N. Fujimura, Y. Morinaga, N. Abe, A. Ashida, T. Ito, *Phys E (Amsterdam)* **10**, 260 (2001)
22. B.B. Li, X.Q. Xiu, R. Zhang, Z.K. Tao, L. Chen, Z.L. Xie, Y.D. Zheng, Z. Xie, *Mater. Sci. Semicond. Proc.* **9**, 141 (2006)
23. E. Liu, P. Xiao, J.S. Chen, B.C. Lim, L. Li, *Curr Appl. Phys.* **8**, 408 (2008)
24. P.K. Sharma, R.K. Dutta, A.C. Pandey, *J. Magn. Magn. Mater.* **321**, 3457 (2009)
25. G.J. Huang, J.B. Wang, X.L. Zhong, G.C. Zhou, H.L. Yan, *J. Mater. Sci.* **42**, 6464 (2007)
26. P.V. Radovanovic, D.R. Gamelin, *Phys. Rev. Lett.* **91**, 157202 (2003)
27. S. Deka, P.A. Joy, *Chem. Mater.* **17**, 6507 (2005)
28. D.R. Gamelin, *J. Am. Chem. Soc.* **124**, 15192 (2002)
29. A.M. Becerra, A.E. Castro-Luna, *J. Chil. Chem. Soc.* **50**, 465 (2005)
30. S.V. Bhat, F.L. Deepak, *Solid State Commun.* **135**, 345 (2005)
31. D.A. Schwartz, K.R. Kittilstved, D.R. Gsaamelin, *Appl. Phys. Lett.* **85**, 1395 (2004)
32. H. Weakliem, *J. Chem. Phys.* **36**, 2117 (1962)
33. C. Li, G. Fang, Q. Fu, F. Su, G. Li, X. Wu, X. Zhao, *J. Crystal Growth* **292**, 19 (2006)
34. Y. Sun, N.G. Ndifor-Angwafor, D.J. Riley, M.N.R. Ashfold, *Chem. Phys. Lett.* **431**, 352 (2006)
35. Z. Fang, Y. Wang, D. Xu, Y. Tan, X. Liu, *Opt. Mater.* **26**, 239 (2004)
36. Y. Dai, Y. Zhang, Y.Q. Bai, Z.L. Wang, *Chem. Phys. Lett.* **375**, 96 (2003)
37. J. Jie, G. Wang, X. Han, Q. Yu, Y. Liao, G. Li, J. Hou, *Chem. Phys. Lett.* **387**, 466 (2004)
38. S.M. Zhou, X.H. Zhang, X. Meng, K. Zou, X. Fan, S. Wu, S.T. Lee, *Nanotechnology* **15**, 1152 (2004)
39. P. Yang, H. Yan, S. Mao, R. Russo, J. Johnson, R. Saykally, N. Morris, J. Phan, R. He, H. Choi, *Adv. Funct. Mater.* **12**, 323 (2002)
40. Z.W. Zhao, B.K. Tay, J.S. Chen, J.F. Hu, B.C. Lim, G.P. Li, *Appl. Phys. Lett.* **90**, 152502 (2007)
41. R.B. Bylisma, W.M. Becker, J. Kossut, U. Debska, D. Yoder-Short, *Phys. Rev. B* **33**, 8207 (1986)
42. Y.R. Lee, A.K. Ramdas, R.L. Aggarwal, *Phys. Rev. B* **38**, 10600 (1988)
43. Y.D. Kim, S.L. Cooper, M.V. Klein, B.T. Jonker, *Phys. Rev. B* **49**, 1732 (1994)